ISSN 0036-0244, Russian Journal of Physical Chemistry A, 2016, Vol. 90, No. 13, pp. 2550–2555. © Pleiades Publishing, Ltd., 2016.

STRUCTURE OF MATTER AND QUANTUM CHEMISTRY

Theoretical Calculations of High-pressure Phases of NiF_2: An Ab Initio Constant-Pressure Study[1]

Cihan Kürkçü[a,*], Ziya Merdan[b], and Hülya Öztürk[a]

[a] *Faculty of Arts and Sciences, Department of Physics, Ahi Evran University, Kırşehir, Turkey*

[b] *Science Faculty, Department of Physics, Gazi University, Ankara, Turkey*

**e-mail: ckurkcu@ahievran.edu.tr, cihankurkcu@gmail.com*

Received August 19, 2015

Abctract—We have studied the structural properties of the antiferromagnetic NiF_2 tetragonal structure with $P4_2/mnm$ symmetry using density functional theory (DFT) under rapid hydrostatic pressure up to 400 GPa. For the exchange correlation energy we used the local density approximation (LDA) of Ceperley and Alder (CA). Two phase transformations are successfully observed through the simulations. The structures of XF_2-type compounds crystallize in rutile-type structure. NiF_2 undergoes phase transformations from the tetragonal rutile-type structure with space group $P4_2/mnm$ to orthorhombic $CaCl_2$-type structure with space group $Pnnm$ and from this orthorhombic phase to monoclinic structure with space group $C2/m$ at 152 GPa and 360 GPa, respectively. These phase changes are also studied by total energy and enthalpy calculations. According to these calculations, we perdict these phase transformations at about 1.85 and 30 GPa.

Keywords: nickel fluoride, ab initio, phase transition, molecular dynamics

DOI: 10.1134/S0036024416130057

I. INTRODUCTION

Because of the novel phase transitions and geophysical importance, the difluoride compounds have been studied under the influence of temperature and pressure [1–9]. NiF_2 compound crystallizes in a tetragonal rutile-type structure (D_{4h}^{14}, $P4_2/mnm$, $Z = 2$) under ambient conditions. Its unit cell consists of two nickel and four fluorine atoms. The nickel (Ni) atoms are located at (0, 0, 0) and $\left(\frac{1}{2}, \frac{1}{2}, \frac{1}{2}\right)$, and fluorine atoms at (x, x, 0), ($-x$, $-x$, 0), $\left(\frac{1}{2}+x, \frac{1}{2}-x, \frac{1}{2}\right)$, and $\left(\frac{1}{2}-x, \frac{1}{2}+x, \frac{1}{2}\right)$, where x has a value about 0.3 and is the only internal coordinate that is not fixed by symmetry. This compound is known as antiferromagnetic at 0 K.

Compounds with this rutile-type structures have received considerable attention for pressure-induced phase transitions [2]. The high-pressure phase transition in NiF_2 was first studied in 1969, by Austin [1] up to 9 GPa. He observed an orthorhombic phase with space group $Pnnm$ for NiF_2. After that, Ming et al. [6] approved that tetragonal rutile-type structure of NiF_2 transform into an orthorhombic $CaCl_2$-type structure at 1.8 GPa at ambient temperature using in situ X-ray diffraction pattern studies.

It is noted that from tetragonal to orthorhombic phase transition has also been observed in some dioxides and fluorides such as FeF_2, CoF_2, CrO_2, SnO_2, ZnF_2, and MgF_2 [10–15]. In spite of structure of XF_2-type (X = Fe, Co, Zn, and Mg) compounds have been extensively studied, the physical mechanism of the tetragonal ($P4_2/mnm$) $\rightarrow$ orthorhombic ($Pnnm$) phase transition has not been obviously determined yet [3]. Solid-to-solid phase transformation driven by pressure shows a very extensive trend that requires a deep theoretical understanding. For these reasons, we decided to study the structures of NiF_2 compound. The mechanisms of these phase transformations at the atomistic level are discussed.

2. COMPUTATIONAL DETAILS

The structural properties of the tetragonal NiF_2 compound are investigated in the local density approximation of density functional theory with the functional of Ceperley and Alder (CA) [16] using the ab-initio program SIESTA [17]. The self-consistent "norm-conserving" pseudopotentials are generated using the Troullier–Martins scheme [18]. The valence atomic configurations used for Ni and F are $3d^8 4s^2$ and $2s^2 2p^5$, respectively. Because the valence electrons are playing a considerable role in the physical properties

[1] The article is published in the original.

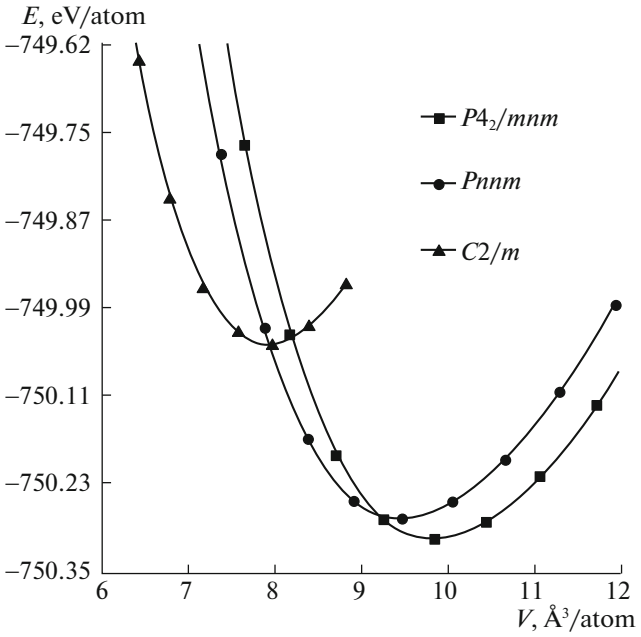

Fig. 1. Energy-volume curves of NiF_2 for $P4_2/mnm$ (—■—), $Pnnm$ (—●—), and $C2/m$ (—▲—) phases.

of the crystals, we take only these electrons of atoms during the calculations. The double-zeta plus polarized orbitals were used in the calculations along with the 150 Ryd mesh cut-off for a real space grid. For the Brillouin zone (BZ) integration, we use the Monkhorst–Pack (MP) [19] mesh 6 × 6 × 8 for rutile-type structure, 8 × 10 × 12 for $CaCl_2$-type structure, and 6 × 6 × 8 for monoclinic structure. The simulation cell consist of 96 atoms with periodic boundary conditions. We employ Γ-point sampling for the BZ integration which is plausible for a simulation cell with 96-atoms. The structures were allowed to relax and to find their equilibrium volumes and lowest energies for each value of the applied pressure by optimizing their lattice vectors and atomic positions together until the maximum atomic forces were getting smaller until 0.01 eV $Å^{-1}$ and the stress tolerances were getting less until 0.5 GPa.

Pressure was applied via the method of conjugate-gradient to the system and increased with an increment of 8 GPa. In order to analyze each minimization step we use the KPLOT program and RGS algorithm [20, 21] that give elaborated knowledge about cell parameters, atomic positions and space group of an analyzed structure.

3. RESULTS AND DISCUSSIONS

The difluorides of the first-row transition metals with tetragonal structures can be produced by a continuous distortion either orthorhombic or monoclinic structures. The experiments revealed phase transitions of NiF_2 under pressure, from the tetragonal rutile-type structure to orthorhombic $CaCl_2$-type structure. The pressure dependence of the phase transition of NiF_2 was investigated. Our study showed that tetragonal structure of NiF_2 transforms to orthorhombic structure, and this orthorhombic structure transforms to monoclinic structure. We first calculated the total energy E_{tot} of rutile-type structure with space group $P4_2/mnm$, $CaCl_2$-type structure with space group $Pnnm$ and monoclinic structure with space group $C2/m$ of NiF_2 and then illustrated in Fig. 1. After that, we make a fit of these energy-volume data to the third-order Birch-Murnaghan equation of state given by

$$P = 1.5B_0\left[(V/V_0)^{-\frac{7}{3}} - (V/V_0)^{-\frac{5}{3}}\right] \times\left\{1 + 0.75(B_0' - 4)\left[(V/V_0)^{-\frac{2}{3}} - 1\right]\right\}, \quad (1)$$

where P is the applied pressure, V is the volume at pressure, V_0, B_0, and B_0' are the volume, bulk modulus

Table 1. Transition pressures, equilibrium lattice parameters, equilibrium volume rates, the bulk modules and their pressure derivatives of $P4_2/mnm$, $Pnnm$, and $C2/m$ phases for NiF_2

Phases	Pressure (GPa)	a (Å)	b (Å)	c (Å)	V (Å)	B_0 (GPa)	B_0'	Reference
$P4_2/mnm$	0	4.6721	4.6721	3.0916	59.10	215	3.5	This study
		4.7170	4.7170	3.0980				[3] (Theory)
		4.7420	4.7420	3.1610				[9] (Theory)
		4.6497	4.6497	3.0836	66.67			[24] (Expt.)
		4.6510	4.6510	3.0480				[25] (Expt.)
$Pnnm$	1.85	5.1623	2.3214	3.0871	37.00	216	3.7	This study
	1.80							[6] (Expt.)
	8.5							[3] (Theory)
$C2/m$	30	4.1463	5.8983	5.0138	122.62	220	4.11	This study

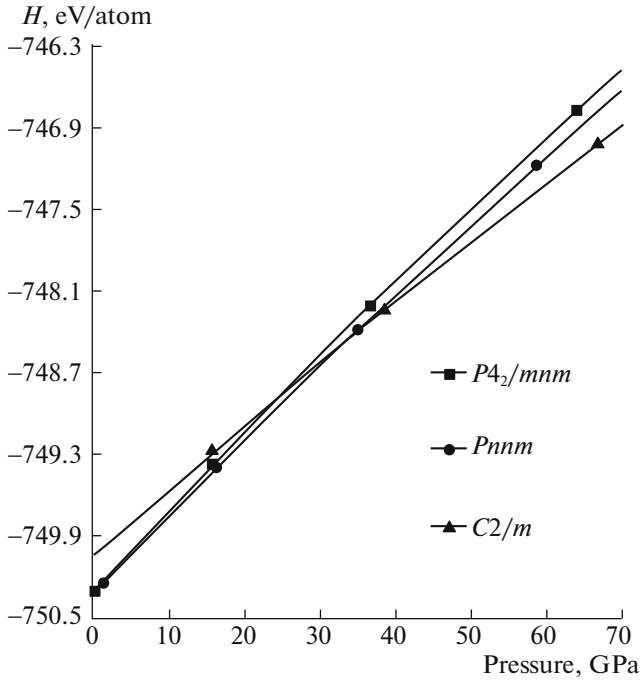

Fig. 2. Enthalpy curves as a function of pressure for $P4_2/mnm$ (—■—), $Pnnm$ (—●—), and $C2/m$ (—▲—) phases.

and its pressure derivative at ambient pressure, respectively [22, 23]. The lattice parameters *a, b, c*, volume *V*, bulk modulus B_0, and its first derivative B_0' obtained from our study at 0, 152, and 360 GPa for $P4_2/mnm$, $Pnnm$, and $C2/m$ phases were given in Table 1, together with other theoretical and experimental results. We used the Gibbs free energy in order to decide the most thermodynamic stable phase at given pressure and temperature. The most stable phase of NiF_2 is $P4_2/mnm$. The Gibbs free energy is described as below:

$$G = E_{tot} + PV - TS, \quad (2)$$

where *E*, *P*, *V*, and *S* are the total energy, pressure, volume and vibrational entropy, respectively. Our theoretical calculations are achieved at 0 K, therefore, the *TS* term is neglected. Thus, Gibbs free energy *G* equals to the enthalpy as follows:

$$H = E_{tot} + PV, \quad (3)$$

where $P = -\partial E_{tot}/\partial V$. As structural phase transitions in the simulations take place across the whole simulation cells, the systems have to cross a noteworthy energy barrier to change from one phase to another one. Therefore the simulated structures should be overpressurized so as to obtain a phase transition. Enthalpy calculations give often reasonable transition pressures relative to experiments. The intersection of two enthalpy curves shows transition pressure. To determine the transition pressure, enthalpy curve is plotted as a function of pressure for rutile structure, $CaCl_2$ structure and monoclinic structure in Fig. 2. We use the energy-volume data for enthalpy calculations. According to these calculations, phase transitions from tetragonal $P4_2/mnm$ phase to orthorhombic $Pnnm$ phase and from orthorhombic $Pnnm$ phase to monoclinic $C2/m$ phase are predicted at pressures of 1.85 and 30 GPa in NiF_2, respectively. Similarly in NiF_2, pressure induced phase transition from $P4_2/mnm$ to $Pnnm$ phase is obtained in the range of 1.8–8.5 GPa [2, 3, 6].

Ni is six-, six-, and nine-fold coordinated by F for the rutile-type structure, $CaCl_2$-type structure, and $C2/m$ phase, respectively. The Ni–F bond lengths range from 1.881 to 1.964 Å and F–F bond lengths range from 2.411 to 2.721 Å for the rutile-type structure. The Ni–F bond lengths range from 1.801 to 1.873 Å and F–F bond lengths range from 2.050 to 2.322 Å for the $CaCl_2$-type structure. The Ni–F bond lengths range from 1.697 to 2.164 Å and F–F bond lengths range from 1.887 to 2.364 Å for the monoclinic structure. The F is three-, three-, and seven- fold coordinated by Ni. The minimum and maximum values of bond lengths and coordination numbers of the $P4_2/mnm$, $Pnnm$, and $C2/m$ phases are given in Table 2.

Table 2. The bond lengths with minimum and maximum values and coordination numbers of the $P4_2/mnm$, $Pnnm$, and $C2/m$ phases. B_{min} and B_{max} indicate minimum and maximum bond lengths, respectively

Phase	From	to	B_{min} (Å)	B_{max} (Å)	Coordination
$P4_2/mnm$	F	Ni	1.881	1.964	F ⇒ [1–3]Ni Ni ⇒ [1–6]F
	F	F	2.411	2.721	F ⇒ [2–9]F
$Pnnm$	F	Ni	1.801	1.873	F ⇒ [1–3]Ni Ni ⇒ [1–6]F
	F	F	2.050	2.322	F ⇒ [2–7]F
$C2/m$	F	Ni	1.697	2.164	F ⇒ [1–5]Ni Ni ⇒ [1–9]F
	F	F	1.887	2.364	F ⇒ [2–7]F

In this study the tetragonal rutile-type structure of NiF_2 was firstly equilibrated at zero pressure and pressure was gradually increased up to 400 GPa with an increment of 8 GPa. The structure of NiF_2 transforms from rutile-type structure with space group $P4_2/mnm$ to $CaCl_2$-type structure with space group $Pnnm$ at 152 GPa and from $CaCl_2$-type structure to monoclinic structure with space group $C2/m$ at 360 GPa. These structures with polyhedral views are depicted in Fig. 3 and their structural parameters and the atomic posi-

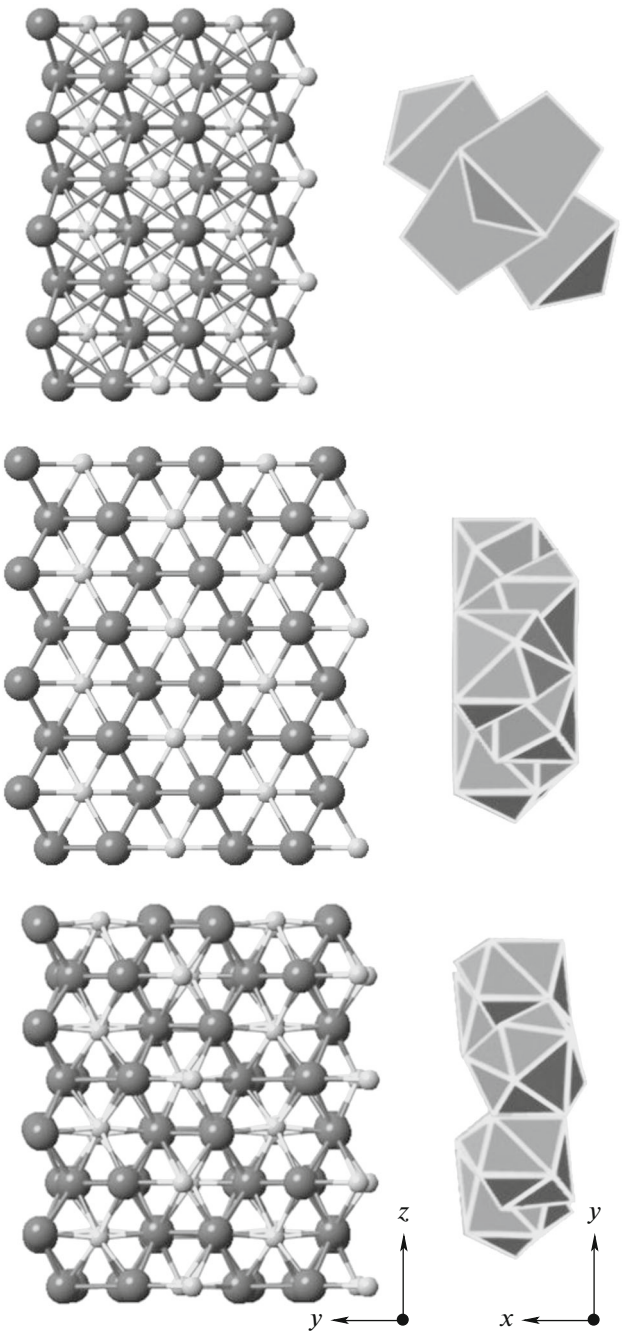

Fig. 3. (Color on-line) Crystal structures with polyhedral views of NiF_2: $P4_2/mnm$ phase at zero pressure (top), *Pnnm* phase at 152 GPa (middle) and $C2/m$ phase at 360 GPa (bottom).

tions are given in Table 3. We plotted volume-pressure relation to determine the thermodynamic nature of the phase transition for NiF_2 in Fig. 4. We can infer that the volume decreases monotonically and the phase transitions are obtained at 152 and 360 GPa. It is clear that the changes in volume are discontinuous at the transition pressures.

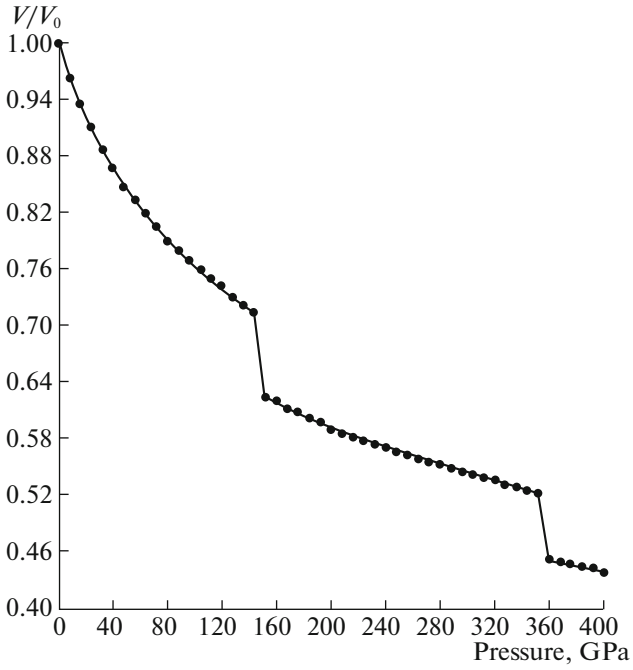

Fig. 4. Volume-pressure relation as a function of pressure for $P4_2/mnm$, *Pnnm*, and $C2/m$ phases.

The cell lengths with **A**, **B**, and **C** and angles with γ, β, and α as a function of minimization step are plotted so as to explain the mechanism of phase transformation. The simulation cell vectors **A**, **B**, and **C** correspond along the [100], [010], and [001] directions in the beginning, respectively. The cell lengths and angles as a function of minimization step are shown at 152 and 360 GPa in Fig. 5.

We attentively analyze the structure each minimization step using the KPLOT program to investigate

Table 3. The equilibrium lattice parameters and the atomic fractional coordinates of the $P4_2/mnm$, *Pnnm*, and $C2/m$ phases

Phases	*a* (Å)	*b* (Å)	*c* (Å)	*x*	*y*	*z*
$P4_2/mnm$	4.6721	4.6721	3.0916	Ni: 0.5000	0.5000	0.5000
				F: 0.1953	0.1953	0.5000
				F: 0.8047	0.8047	0.5000
Pnnm	5.1623	2.3214	3.0871	Ni: 0.5000	0.5000	0.5000
				F: 0.1676	0.7371	0.5000
				F: 0.8324	0.2629	0.5000
$C2/m$	4.1463	5.8983	5.0138	Ni: 0.5000	0.7324	0.0000
				F: 0.4005	0.7598	0.6676
				F: 0.9005	0.2598	0.6676

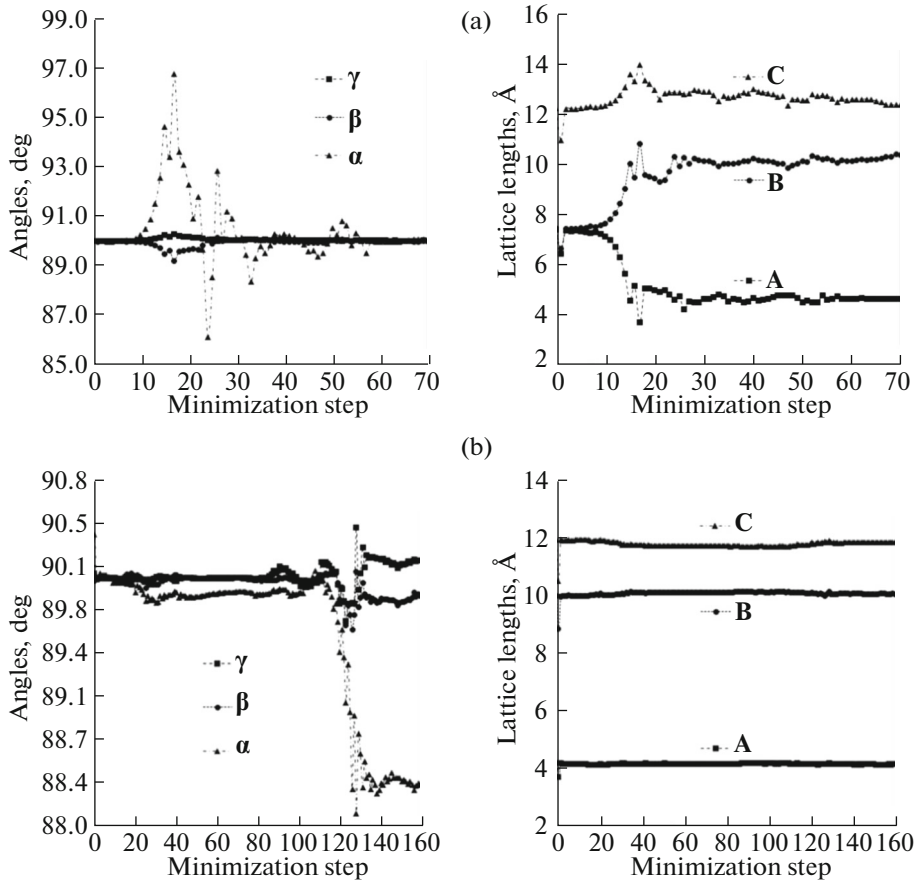

Fig. 5. The simulation cell lengths and angles as a function of the MD time step at (a) 152 and (b) 360 GPa for NiF_2.

whether there is any intermediate phase during the phase transition or not. We didn't find any intermediary phase.

4. CONCLUSION

In this work, the phase transition mechanism of NiF_2 was theoretically studied under pressure up to 400 GPa with an increment of 8 GPa. The structures of NiF_2 were analyzed with KPLOT program. We obtained phase transitions from tetragonal rutile-type structure with space group $P4_2/mnm$ to orthorhombic $CaCl_2$-type structure with space group $Pnnm$ at 152 GPa and another phase transition from $CaCl_2$-type structure to monoclinic structure with space group $C2/m$ at 360 GPa. These structures have 6, 6, and 24 atoms per unit cell. Ni is six-, six- and nine-fold coordinated by F, and F is three-, three- and five-fold coordinated by Ni for the rutile-type structure, $CaCl_2$-type structure and monoclinic structure, respectively. As far as we know, monoclinic phase of NiF_2 has not been found in any previous studies.

REFERENCES

1. A. E. Austin, J. Phys. Chem. Solids **30**, 1282 (1969).
2. J. D. Jorgensen, T. G. Worlton, and J. C. Jamieson, Phys. Rev. B **17**, 2212 (1978).
3. H. Wang, X. Liu, Y. Li, Y. Liu, and Y. Ma, Solid State Commun. **151**, 1475 (2011).
4. A. Y. Wu, Phys. Lett. A **60**, 260 (1977).
5. J. C. Jamieson and A. Y. Wu, J. Appl. Phys. **48**, 4573 (1977).
6. L. C. Ming, M. H. Manghnani, T. Matsui, and J. C. Jamieson, Phys. Earth Planet. Inter. **23**, 276 (1980).
7. L. Nagel and M. O'Keeffe, Mater. Res. Bull. **6**, 1317 (1971).
8. P. Duffek, K. Schwarz, and P. Blaha, Phys. Rev. B **48**, 12672 (1993).
9. I.de P. R. Moreira, R. Dovesi, C. Roetti, V. R. Saunders, and R. Orlando, Phys. Rev. B **62**, 7816 (2000).
10. S. Lopez-Moreno, A. H. Romero, J. Mejia-Lopez, A. Munoz, and I. V. Roshchin, Phys. Rev. B **85**, 134110 (2012).
11. J. A. Barreda-Argüeso, S. Lopez-Moreno, M. N. Sanz-Ortiz, F. Aguado, R. Valiente, J. Gonzalez, F. Rodriguez, A. H. Romero, A. Munoz, L. Nataf, and F. Baudelet, Phys. Rev. B **88**, 214108 (2013).

12. H. Y. Wu, Y. H. Chen, C. R. Deng, and X. F. Su, Phase Trans. **85**, 708 (2012).
13. I. Erdem, H. H. Kart, and T. Cagin, J. Alloys Comp. **587**, 638 (2014).
14. W. J. Bang, C. X. Lu, Z. Hong, and X. Z. Wei, Chin. Phys. B **23**, 077102 (2014).
15. H. Ozturk, C. Kurkcu, and C. Kurkcu, J. Alloys Comp. **597**, 155 (2014).
16. D. M. Ceperley and B. J. Adler, Phys. Rev. Lett. **45**, 566 (1980).
17. P. Ordejon, E. Artacho, and J. M. Soler, Phys. Rev. B **53**, R10441 (1996).
18. N. Troullier and J. L. Martins, Phys. Rev. B **43**, 1993 (1991).
19. H. J. Monkhorst and J. D. Pack, Phys. Rev. B **13**, 5188 (1976).
20. R. Hundt, J. C Schön, A. Hanneman, and M. Jansen, J. Appl. Cryst. **32**, 413 (1999).
21. A. Hannemann, R. Hundt, J. C. Schön, and M. Jansen, J. Appl. Cryst. **31**, 922 (1998).
22. F. Birch, Phys. Rev. **71**, 809 (1947).
23. F. D. Murnaghan, Proc. Natl. Acad. Sci. USA **30**, 244 (1944).
24. M. M. R. Costa, J. A. Paixao, M. J. M. de Almeida, and L. C. R. Andrade, Acta Crystallogr. B **49**, 591 (1993).
25. D. Gerlich, S. Hart, and D. Whittal, Phys. Rev. B **29**, 2142 (1984).